

Robustness against Disorder of Relativistic Spectral Properties in Chalcogenide Alloys

Domenico Di Sante,^{1,2} Paolo Barone,¹ Evgeny Plekhanov,¹ Sergio Ciuchi,^{2,3} and Silvia Picozzi¹

¹*Consiglio Nazionale delle Ricerche (CNR-SPIN), Via Vetoio, L'Aquila, Italy*

²*Department of Physical and Chemical Sciences,*

*University of L'Aquila, Via Vetoio 10, I-67010 L'Aquila, Italy**

³*Consiglio Nazionale delle Ricerche (CNR-ISC), Via dei Taurini, Rome, Italy*

(Dated: February 28, 2022)

In order to carefully address the interplay between substitutional disorder and spin-orbit-coupling in IV-VI alloys, we propose a novel theoretical approach that integrates the reliability of plane-wave based density-functional theory beyond the local-density approximation with the Coherent Potential Approximation. By applying the proposed method to ternary chalcogenide alloys, we predict a substantial robustness of spectral features close to the Fermi energy against substitutional disorder. Supplementing our first-principles calculations with the analysis of the $k \cdot p$ model for rock-salt chalcogenides, we show that the disorder self-energy is vanishingly small close to the band gap, thus allowing for bulk Rashba-like spin splitting to be observed in ferroelectric alloys, such as $\text{PbS}_x\text{Te}_{1-x}$, and protecting the band-character inversion related to the topological transition in the recently discovered Topological Crystalline Insulator $\text{Pb}_{1-x}\text{Sn}_x\text{Te}$.

PACS numbers: 73.20.At,71.23.-k,74.62.En

Introduction. It is nowadays well accepted that spin-orbit coupling (SOC) lies at the origin of a rich variety of appealing phenomenologies, ranging from topological insulators (TI) [1, 2], showing fully spin-polarized metallic surface states despite their bulk insulating character, to large bulk Rashba-like spin-splitting effects in non-centrosymmetric and polar materials [3–5], characterized by strong spin-momentum locking and spin-polarized bands. In this respect, the long-known class of main-group IV-VI semiconducting chalcogenides is playing a key role. On one hand, SnTe has been proposed[6], and later confirmed[7], to belong to a new class of TI with unique features arising from the combination of time-reversal and crystalline symmetries, hence named Topological Crystalline Insulators (TCIs)[8, 9]. On the other hand, GeTe — one of the few known ferroelectric semiconductors — has been put forward as the first example of so-called Ferroelectric Rashba Semiconductors (FER-SCs) with large Rashba splitting[10], where the possibility to permanently control its spin texture via a switchable electric polarization could introduce new functionalities in spintronic devices[5]. In principle, bulk Rashba-like effects and topological features could even be realized within the same material. As a matter of fact, SnTe itself undergoes a low-temperature ferroelectric (FE) transition under certain conditions[11], whose potential implications on its TCI phase have been recently theoretically investigated[12]. The potential relevance of noncentrosymmetric TI with Rashba-like spin-splitting has been also proposed for the acentric semiconductors BiTeI under pressure[13] and BiTeCl [4].

Beside GeTe and SnTe , FE transitions have been reported in several ternary or quaternary alloys of rock-salt IV-VI chalcogenides, such as $\text{Pb}_{1-x}\text{Ge}_x\text{Te}$, $\text{Pb}_{1-x}\text{Sn}_x\text{Te}$ and $\text{PbS}_x\text{Te}_{1-x}$ [14–16]. Similarly, TCI features have

been observed in photoemission (ARPES) spectra of n-type $\text{Pb}_{1-x}\text{Sn}_x\text{Te}$ and p-type $\text{Pb}_{1-x}\text{Sn}_x\text{Se}$ alloys as a function of doping [17–22]. When addressing the relativistic properties of such alloys, due to the intrinsically disordered character of the solid-state solution, a major issue appears. While the role of disorder in \mathcal{Z}_2 TI has been extensively investigated[23–25], showing that time-reversal symmetry guarantees the presence of metallic edge states, topologically protected from non-magnetic impurities, it is not obvious how disorder entangles with spin-orbit in TCI alloys, since crystalline symmetries, crucial for topological properties, are locally broken in a random way. On the basis of general arguments, delocalized states were shown to survive at the surface of TCIs as long as the relevant symmetries, which are broken by disorder, are restored by disorder averaging, analogously to what happens in weak \mathcal{Z}_2 TI[26]. However, signatures of disorder should manifest in the ARPES spectra[22]. Similarly, broadening/smearing effects induced by disorder could in principle screen, reduce or even prevent any bulk Rashba-type spin-splitting in FE alloys.

In this Letter, we investigate the role of disorder in the relativistic electronic properties of IV-VI chalcogenide ternary alloys by interfacing a Coherent-Potential-Approximation (CPA) approach[27] to highly accurate density-functional theory (DFT) relativistic calculations. Aiming at a quantitative analysis of the effect of disorder in the spectral features of such alloys, we calculate the disorder self-energy in the CPA framework, using, as a starting point, accurate DFT calculations on ordered binary compounds based on the HSE hybrid functional, as implemented in VASP [28–30]. Demanding hybrid-functional calculations have been shown to provide, in good agreement with GW calculations[31, 32], the correct band ordering at the valence band maximum

(VBM) and conductance band minimum (CBM) in all lead chalcogenides, at variance with severe failures within local-density approximation. This issue is of dramatic importance in rock-salt chalcogenides, where a band-character inversion at the high-symmetry L point drives the topological transition, with a change in the mirror Chern number by two[6, 9]. Ab-initio relativistic HSE band structures are then projected onto a Wannier basis set [33], and Wannier-functions tight-binding parameters are used for the CPA self-consistency loops (see details in [34]). We stress that, to the best of our knowledge, this is the first time that such hybrid DFT-CPA approach is used in the study of disordered systems, hopefully providing an alternative approach to well-established techniques, such as the fully relativistic KKR-CPA[35–37], often based on local-density approximation. Our approach also allows to tailor disorder effects in the surface states of alloys without resorting to computationally demanding DFT supercell calculations, at the same time improving on the conventional methodology, where tight-binding Hamiltonians are built up in slab geometry. In the latter approach, substitutional disorder in TCI chalcogenide alloys has been so far taken into account within the Virtual Crystal Approximation (VCA)[19], where no self-energy correction accounting for the effective disorder interaction is included. On the other hand, the spectral features of the surface states are encoded in the Surface Single-site Green’s Function, which can be easily calculated from the DFT-CPA single-site disorder-averaged Green’s Function using an iterative surface renormalization method in the limit of a semi-infinite slab[34, 38].

On the grounds of our newly developed methodology, we focus on two ternary alloys, $\text{PbS}_x\text{Te}_{1-x}$ and $\text{Pb}_{1-x}\text{Sn}_x\text{Te}$, showing that the former belongs to the class of FERSC, where a large Rashba-like spin-splitting develops in disordered FE alloys, while we provide a microscopic analysis of the topological nature of the TCI phase that develops in the latter.

Application to PbSTe FERSC alloy. We first focus on the interplay between disorder and Rashba-type spin splittings in FE $\text{PbS}_x\text{Te}_{1-x}$ [15, 16]. The pristine compounds PbTe and PbS don’t display any FE instability, both crystallizing in the centrosymmetric face-centered cubic structure. On the other hand, their alloys, up to a sulfur concentration of $x_c \sim 0.45$, show FE phase transitions at doping-dependent Curie temperatures, displaying a maximum $T_c \sim 80\text{ K}$ around $x = 0.18$ [16]. By means of EXAFS, the origin of such transition has been ascribed to the off-centering of S ions in a substantially centrosymmetric PbTe host[15], due to different size and polarizability of S and Te ions. Our DFT supercell calculations confirm this scenario, finding that below a critical concentration $x_c \sim 0.4$ sulfur displacements vary in the same range that has been experimentally observed, whereas only Te ions close to S are slightly displaced (see details in [34]).

At the FE transition, the alloy structure changes from cubic to distorted rhombohedral (space group $R3m$), being thus isostructural with the prototypical Ferroelectric Rashba Semiconductor GeTe[5]. Rashba-like spin splittings are therefore expected to develop in the presence of SOC, especially at the VBM and CBM around the high-symmetry point Z, at the center of the hexagonal faces in the Brillouin zone (BZ) which are perpendicular to the [111] polar axis[5], provided disorder-induced broadening effects do not overcome such tiny features of the spectral function. Indeed, strong signatures of the random S/Te substitution appear, especially in the valence bands with predominant anionic character, as shown in Fig. 1a). Nonetheless, *the smearing of the spectral function is substantially reduced around the Fermi level*. Remarkably, we find that the VBM and CBM are more robust against disorder renormalization as the band gap decreases. In fact, the disorder self-energy appears to depend not only on the nominal S/Te concentration, but also on the size of the gap, which in turn is loosely proportional to the

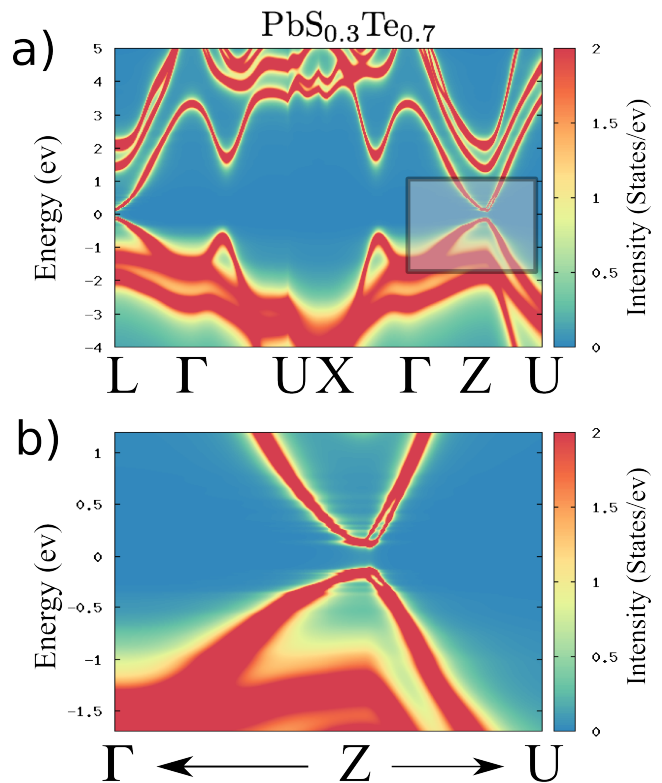


FIG. 1: (Color online) (a) DFT(HSE)+CPA Spectral Function for $\text{PbS}_{0.3}\text{Te}_{0.7}$ FE alloy along the full irreducible rhombohedral BZ, where a clear spin-splitting signature appears in the black rectangle. (b) Zoom of the spectral function around the Z point, corresponding to the black rectangle in panel (a), highlighting a Rashba-like induced spin-splitting of about 50 meV along the ZU line perpendicular to the polar axis.

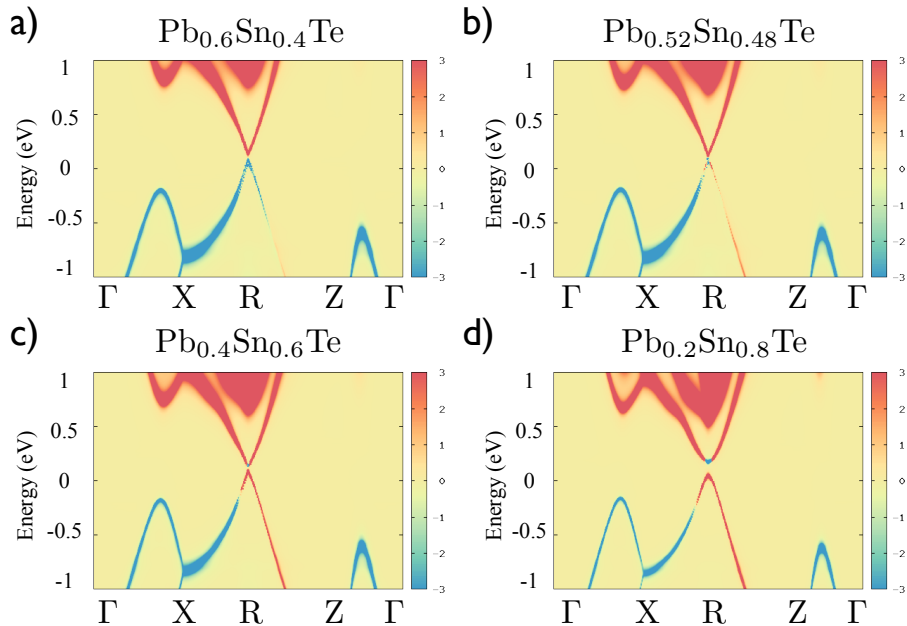


FIG. 2: (Color online) DFT(HSE)+CPA evolution of $\text{Pb}_{1-x}\text{Sn}_x\text{Te}$ alloy spectral features as a function of Sn concentration for $x=0.4, 0.48, 0.6$ and 0.8 in a), b), c) and d) panels respectively, along the irreducible tetragonal BZ. Red (positive) values refer to the spectral function $A(\mathbf{k}, \omega) = -\text{ImTr}\mathcal{G}(\mathbf{k}, \omega)/\pi$ projected on the $\text{Pb}_{1-x}\text{Sn}_x$ cation, while blue (negative) values are projection of the spectral function on the Te anion. The R point is the projection of the rhombohedral L point on the tetragonal BZ.

amount of S off-centering. Since the latter decreases as the S concentration increases above $x \sim 0.18$, spin-splitting signatures become clearly visible due to the smaller disorder self-energy, as shown in Fig. 1b) for $x = 0.3$. On the other hand, for small S concentrations such splitting effects are substantially depressed, virtually disappearing, by disorder renormalization effects, despite the nominally weaker substitutional disorder. We stress the fact that our DFT+CPA approach is essential in capturing such disorder-induced renormalization effects. As a matter of fact, a VCA approach — not taking into account the disorder self-energy — would predict large spin splittings for all concentrations corresponding to the FE phase (see details in Suppl. Mat. [34]). Being isostructural with FE GeTe and SnTe, our results suggest that novel FERSC materials, allowing for the control and manipulation of Rashba-like spin textures by tuning the FE polarization[5, 10], could be identified in the broad class of chalcogenide alloys. Depending on doping concentration, tiny features of ARPES spectra could become visible in $\text{PbS}_x\text{Te}_{1-x}$ or related $\text{PbSe}_x\text{Te}_{1-x}$ [16], as the self-energy induced by substitutional disorder may be significantly reduced close to the Fermi energy.

Application to PbSnTe TCI alloy. We turn now to the study of the well known topological transition as a function of tin concentration in the $\text{Pb}_{1-x}\text{Sn}_x\text{Te}$ alloy. This compound, along with the analogue $\text{Pb}_{1-x}\text{Sn}_x\text{Se}$,

has been intensively studied, both experimentally and theoretically [17–22]. For the first time, we propose in this Letter an ab-initio analysis of the disorder effects on its spectral features by calculating the disorder self-energy in our combined DFT-CPA framework. In Fig. 2, we show the anion/cation resolved spectral functions for different dopings. The CPA approach clearly describes the doping-induced band closure at the L points (R points in the tetragonal setting), implying a change of the alloy topological character, with a critical tin concentration $x_c \sim 0.48$ [39]. As a consequence of the cation Pb/Sn substitution, disorder effects are more visible at positive energies with respect to the Fermi level, i.e. where states have a predominant cationic orbital character. The presence of disorder is reflected in the significant broadening of the spectral features (spectra in wider energy windows are reported in Supplementary Material[34]), as a consequence of a larger self-energy. However, approaching the Dirac point — where bands show an almost linear behavior — the spectral broadening vanishes, and a clear signature of character inversion is visible. Remarkably, such inversion appears to be protected against disorder, since the imaginary part of the disorder self-energy is found to vanish. As a result, *bands are not renormalized (broadened) by the interaction with disorder around the bulk Dirac point.*

The trivial/topological nature of the bulk band-

structure is reflected in the lack/presence of metallic surface states through the bulk-boundary correspondence principle[2]. In particular, an inverted orbital cation/anion character in the rock-salt chalcogenides ensures the appearance of Dirac-like surface states[6]. In fact, we find that gapless surface states appear as the tin concentration overcomes the critical value $x_c \sim 0.48$ (for a trend of the surface spectral function as a function of doping see the Supplementary Material [34]). The case of $\text{Pb}_{0.2}\text{Sn}_{0.8}\text{Te}$ TCI alloy is shown in Fig. 3, where a surface Dirac cone located close to the \bar{X} (as in pristine SnTe[6]) is clearly visible. As it happens in the bulk band-structure, surface states appear to be well protected against disorder-induced broadenings around the Dirac point. We emphasize that surface spectral functions calculated within our approach find a direct link with experimental ARPES spectra, apart from matrix element effects (see e.g. Refs[17, 19, 22]).

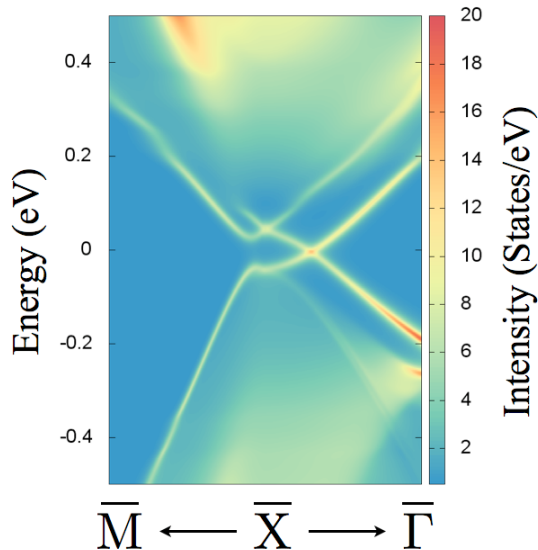


FIG. 3: (Color online) DFT(HSE)+CPA Surface Spectral Function for $\text{Pb}_{0.2}\text{Sn}_{0.8}\text{Te}$ TCI alloy (see Fig. 2d for the bulk spectral function). The k-axis show 1/10 of the $\bar{M} - \bar{X}$ and $\bar{X} - \bar{\Gamma}$ lines around \bar{X} .

CPA on the $k \cdot p$ model for TCI. The origin of the Dirac-point protection against substitutional disorder can be further analyzed by considering the CPA description of a trivial/topological alloy in the framework of $k \cdot p$ model. The band structure of rock-salt chalcogenides around the L points is given by[6, 40]:

$$\hat{H}^{\pm} = \pm m\sigma_z + \nu(k_1s_2 - k_2s_1)\sigma_x + \nu'k_3\sigma_y, \quad (1)$$

where $\mathbf{k} = (k_1, k_2, k_3)$ forms an orthogonal system with k_3 parallel to the ΓL direction and k_1 along the direction perpendicular to a mirror plane. Hamiltonian (1) is represented in the basis of cation and anion p-orbitals p_c/p_a ($\sigma_z = \pm 1$) and total angular momentum along ΓL $j = \pm 1/2$ ($s_3 = \pm 1$). ν and ν' are materials-dependent

parameters. The plus/minus sign in front of the mass term m refers to the trivial/topological insulator with direct/inverted band character at the gap[6]. The CPA description of the trivial/topological material alloy is based on the single-site disordered-averaged propagator:

$$\hat{\mathcal{G}}(\omega) = x[\hat{G}_0(\omega)^{-1} - \hat{H}^+]^{-1} + (1-x)[\hat{G}_0(\omega)^{-1} - \hat{H}^-]^{-1}, \quad (2)$$

with \hat{H}^{\pm} being the local (k-independent) part of Hamiltonian (1) and \hat{G}_0 being the local propagator which embodies the average action of the environment. The disorder self-energy ($\hat{\Sigma}(\omega)$) defined as

$$\hat{\mathcal{G}}(\omega) = [\hat{G}_0(\omega)^{-1} - \hat{\Sigma}(\omega)]^{-1} \quad (3)$$

contains all information relative to the role played by disorder. All the detailed CPA calculations are extensively given in the Supplementary Material [34]; here we will focus only on the most relevant results. At the critical concentration x_c where the bulk gap closes with bands linearly dispersing, the disorder self-energy can be written as $\Sigma(\omega) = -a\omega - ib\omega^2$ with $a \sim m^2/\Gamma^2$ and $b \sim m^2/\Gamma^3$, where Γ is a high energy cut-off naturally introduced when dealing with linearized models[41]. The density of states $N(\omega) = -\text{Im}\mathcal{G}(\omega)/\pi$ assumes the simple parabolic expression $N(\omega) = 3\omega^2/2\Gamma^3$ coming from the tridimensionality of the Dirac cone. Remarkably, the imaginary part of the disorder self-energy, which is related to the finite life-time and bandwidth of electronic states, goes monotonically to zero when approaching the Dirac point ($\omega = 0$), vanishing at the Fermi level. This is of fundamental importance for the anion/cation band character inversion related to the topological transition[6], since the energy region of interest for the orbital character inversion around the L points is protected against disorder-induced broadening effects. Interestingly, such a protection is absent in graphene, where a non vanishing self-energy at the Fermi level leads to the so-called universal conductivity (see details in [34]). It is also worth to note here that our results for the 3D Dirac cone at the trivial/topological transition show many similarities with those obtained for Weyl electron systems and three dimensional \mathcal{Z}_2 topological insulators in the weak conformational disorder limit [42–44]. On the other hand, it is important to highlight that finite-range potential disorder, as well as spatial correlations, beyond CPA, taken into account by Dynamical Cluster Approximation, can lead to an exponentially small density of states at the Dirac point, as a direct consequence of a small, but finite, disorder self-energy at the Fermi level [45, 46].

Conclusions: In this work we've addressed the crucial role of substitutional disorder in the class of IV-VI chalcogenides, featuring SnTe and GeTe as binary prototypes of TCIs and FERSC, respectively. The main outcome of our theoretical analysis, based on the CPA model and ab-initio calculations, is the prediction that spectral

features in proximity to the Fermi level are robust with respect to substitutional disorder. In closer detail, we predict a strong interplay between disorder and Rashba spin-splittings in ferroelectric $\text{PbS}_x\text{Te}_{1-x}$ ternary alloys. Moreover, in $\text{Pb}_{1-x}\text{Sn}_x\text{Te}$ we find that, as the disorder-induced self-energy vanishes at the bulk Dirac point, the orbital character inversion - “smoking gun” of the topological transition - is protected against the effects of disorder. As a result, the spectral features of the Dirac-like conducting surface states are robust and therefore clearly detectable in experiments.

We kindly acknowledge A. Narayan and K. Palotas for useful discussions. We acknowledge CINECA for awarding us access to Fermi supercomputer and the CARIPLO Foundation through the MAGISTER project Rif. 2013-0726.

* Electronic address: domenico.disante@aquila.infn.it

- [1] M. Z. Hasan and C. L. Kane, *Rev. Mod. Phys.* **82**, 3045 (2010).
- [2] X. L. Qi and S. C. Zhang, *Rev. Mod. Phys.* **83**, 1057 (2011).
- [3] K. Ishizaka et al., *Nat. Mater.* **10**, 521 (2011).
- [4] Y. L. Chen, M. Kanou, Z. K. Liu, H. J. Zhang, J. A. Sobota, D. Leuenberger, S. K. Mo, B. Zhou, S.-L. Yang, P. S. Kirchmann, et al., *Nature Phys.* **9**, 704 (2013).
- [5] D. Di Sante, P. Barone, R. Bertacco, and S. Picozzi, *Adv. Mater.* **25**, 509 (2013).
- [6] T. H. Hsieh, H. Lin, J. Liu, W. Duan, A. Bansil, and L. Fu, *Nat. Commun.* **3**, 982 (2012).
- [7] Y. Tanaka, Z. Ren, T. Sato, K. Nakayama, S. Souma, T. Takahashi, K. Segawa, and Y. Ando, *Nature Phys.* **8**, 800 (2012).
- [8] L. Fu, *Phys. Rev. Lett.* **106**, 106802 (2011).
- [9] R. J. Slager, A. Mesaros, V. Juričić, and J. Zaanen, *Nat. Phys.* **9**, 98 (2013).
- [10] S. Picozzi, *Front. Physics* **2**, 10 (2014).
- [11] K. L. S. Kobayashi, Y. Kato, Y. Katayama, and K. F. Komatsubara, *Phys. Rev. Lett.* **37**, 772 (1976).
- [12] E. Plekhanov, P. Barone, D. Di Sante, and S. Picozzi (2014), arXiv:1402.2574.
- [13] S. Bahramy, B. J. Yang, R. Arita, and N. Nagaosa, *Nat. Commun.* **3**, 679 (2012).
- [14] M. E. Lines and A. M. Glass, eds., *Principles and Applications of Ferroelectrics and Related Materials* (Clarendon Press, Oxford, 1977).
- [15] Z. Wang and B. A. Bunker, *Phys. Rev. B* **46**, 11277 (1992).
- [16] A. I. Lebedev and I. A. Sluchinskaya, *Ferroelectrics* **157**, 275 (1994).
- [17] S.-Y. Xu, C. Liu, N. Alidoust, et al., *Nat. Commun.* **3**, 1192 (2012).
- [18] Y. Tanaka, T. Sato, K. Nakayama, S. Souma, T. Takahashi, Z. Ren, M. Novak, K. Segawa, and Y. Ando, *Phys. Rev. B* **87**, 155105 (2013).
- [19] P. Dziawa, B. Kowalski, K. Dybko, et al., *Nat. Mat.* **11**, 1023 (2012).
- [20] B. M. Wojek, R. Buczko, S. Safaei, P. Dziawa, B. J. Kowalski, M. H. Berntsen, T. Balasubramanian, M. Leandersson, A. Szczerbakow, P. Kacman, et al., *Phys. Rev. B* **87**, 115106 (2013).
- [21] C. M. Polley, P. Dziawa, A. Reszka, A. Szczerbakow, R. Minikayev, J. Z. Domagala, S. Safaei, P. Kacman, R. Buczko, J. Adell, et al., *Phys. Rev. B* **89**, 075317 (2014).
- [22] B. M. Wojek, P. Dziawa, B. J. Kowalski, A. Szczerbakow, A. M. Black-Schaer, M. H. Berntsen, T. Balasubramanian, T. Story, and O. Tjernberga (2014), arXiv:1401.6643.
- [23] B. Leung and E. Prodan, *Phys. Rev. B* **85**, 205136 (2012).
- [24] T. Morimoto and A. Furusaki, *Phys. Rev. B* **89**, 035117 (2014).
- [25] A. Narayan, I. Rungger, and S. Sanvito, *Phys. Rev. B* **86**, 201402 (2012).
- [26] L. Fu and C. L. Kane, *Phys. Rev. Lett.* **109**, 246605 (2012).
- [27] P. Soven, *Phys. Rev.* **156**, 809 (1967).
- [28] J. Heyd, G. E. Scuseria, and M. Ernzerhof, *J. Chem. Phys.* **121**, 1187 (2004).
- [29] G. Kresse and J. Furthmüller, *Phys. Rev. B* **54**, 11169 (1996).
- [30] Kohn-Sham equations were solved using the projector augmented-wave method. The energy cutoff for the plane-wave expansion was 600 eV; an 8x8x8 Monkhorst-Pack k-point grid was used.
- [31] K. Hummer, A. Grüneis, and G. Kresse, *Phys. Rev. B* **75**, 195211 (2007).
- [32] A. Svane, N. E. Christensen, M. Cardona, A. N. Chantis, M. van Schilfgaarde, and T. Kotani, *Phys. Rev. B* **81**, 245120 (2010).
- [33] A. A. Mostofi, J. R. Yates, Y.-S. Lee, I. Souza, D. Vanderbilt, and N. Marzari, *Comput. Phys. Commun.* **178**, 685 (2008).
- [34] See Supplementary Material (link added by the journal).
- [35] H. Ebert, D. Ködderitzsch, and J. Minár, *Rep. Prog. Phys.* **74**, 096501 (2011).
- [36] S. Chadov, J. Kiss, J. Kübler, and C. Felser, *Phys. Status Solidi RRL* **1**, 82 (2013).
- [37] G. M. Stocks, W. M. Temmerman, and B. L. Gyorffy, *Phys. Rev. Lett.* **41**, 339 (1978).
- [38] J. Henk and W. Schattke, *Computer Physics Communications* **77**, 69 (1993).
- [39] The agreement with experiment can be further improved performing the hybrid functional calculations not at the PbTe and SnTe equilibrium lattice constant but at the lattice constant of the alloy.
- [40] D. L. Mitchell and R. F. Wallis, *Phys. Rev.* **151**, 581 (1966).
- [41] Inclusion of a small gaussian conformational disorder with variance $\sigma \ll m$ causes only a renormalization of coefficients a and b , where m is replaced with $(m^2 + \sigma^2)$ [34].
- [42] Y. Ominato and M. Koshino, *Phys. Rev. B* **89**, 054202 (2014).
- [43] E. J. B. S. Sbierski, G. Pohl and P. W. Brouwer (2014), arXiv:1402.6653.
- [44] K. Kobayashi, T. Ohtsuki, K.-I. Imura, and I. F. Herbut, *Phys. Rev. Lett.* **112**, 016402 (2014).
- [45] R. Nandkishore, D. A. Huse, and S. L. Sondhi, *Phys. Rev. B* **89**, 245110 (2014).
- [46] M. Jarrell and H. R. Krishnamurthy, *Phys. Rev. B* **63**, 125102 (2001).